Demonstration of a Bidirectional Coherent Air-to-Ground Optical Link

C. Chen, A. Grier, M. Malfa, E. Booen, H. Harding, C. Xia, M. Hunwardsen, J. Demers, K. Kudinov, G. Mak, B. Smith, A. Sahasrabudhe, F. Patawaran, T. Wang, A. Wang, C. Zhao, D. Leang, J. Gin, M. Lewis, B. Zhang, D. Nguyen, D. Jandrain*, F. Haque, and K. Quirk
Facebook Inc., 1 Hacker Way, Menlo Park, CA 94025
*Averna Technologies Inc., 87 Prince St., Montreal, Québec, Canada H3C 2M7

ABSTRACT

Coherent, free-space optical communication technology offers near-quantum-limited receiver sensitivity and high spectral efficiency compared to conventional direct detection systems. In this paper, we will present the initial results from a bidirectional air-to-ground demonstration of a coherent optical link.

Keywords List: Free Space Optics, Laser Communications, UAV, Pointing and Tracking, Atmospheric Propagation, Connectivity Lab

1 INTRODUCTION

Facebook has been exploring the possible use of solar-powered unmanned autonomous vehicles (UAVs) as platforms for continuous internet delivery for populations that live beyond the reach of terrestrial connectivity. High capacity laser communications (lasercom) crosslinks between UAV platforms could provide backbone connectivity and network redundancy to a UAV network. To operate effectively as a backbone network, the capacity of the crosslink needs to be several times the data capacity of a single node, which for most studies has a data capacity of 10's of gigabits per second (Gbps). At this data rate and link range, lasercom technology has advantages compared to mm-wave-based solutions. The small size of the aperture reduces the size of the radome and hence the drag on the UAVs. Flying at an altitude of 18-25 km, the lasercom link stays above the cloud layers even with link range on the order of 250-300 km, and can operate with very high link availability. Finally, since the projected bandwidth growth of typical data traffic is expected to increase rapidly, laser crosslinks, given the capacity to multiplex additional wavelengths, can provide a seamless upgrade path to higher data capacity without fundamentally changing the design of the optical front end.

The design of the UAV crosslink terminal is similar to those intended for other-long range applications, e.g. space. However, the payload does not have to accommodate the severe vibration environment of the space launch, enabling the use of commercial design components. Unlike space lasercom links where the two terminals are moving at high relative velocity, forcing the transmit signal to point ahead of the receive line of sight, lasercom links based on UAV platforms can use a single fiber for both transmit and receive and allow for a simpler optical design. The ability for the UAV payload to be recovered and refurbished also implies reduced redundancy and reliability requirements. Finally, the ability to upgrade the equipment allows for continuous updates to the design as new capabilities emerge.

Designing a lasercom terminal for the UAV environment has its own unique set of challenges. The need to stay aloft continuously for long periods of time, even in adverse solar illumination conditions, for example flying in winter, limits the maximum payload weight that can be carried by the plane. The need to store enough energy to power the platform and the payloads imposes a power consumption ceiling on the payloads. Our initial design goal is to accommodate multiple payloads within a 25-kg, 250-W allocation. The aerodynamic drag of the optical payload is also an important consideration for efficient flight and generally favors payloads with a small exposed cross section. Furthermore, the thermal conditions that the payload needs to accommodate can easily exceed the ambient condition of a typical space payload environment. At altitudes of 18-25 km, the external environment can range from -29 to -88 C. Thermal management techniques, such as survival heaters and radiators, used by space payloads generally add weight or power consumption that are not desirable for a UAV applications.

In this paper, we present the initial testing results of a UAV lasercom payload in an air-ground condition. Section 2 describes the link design for both air-air and air-ground engagements. The designs of the air- and ground-terminals are described in Sections 3 and 4, respectively. Results of the lab test and flight tests are summarized in Section 5.

2 AIR-GROUND LINK DESIGN

As part of the backbone network, the link should support a data rate that is several times the individual node's capacity. Furthermore, as recent internet usage trends indicate, the data demand for the system will continue to grow rapidly over the next few years. Therefore, the communications technology selected must be expandable to address future needs. For this reason, we elected to implement a system with fiber-coupled backend. Such a system allows to increase the link capacity by simply adding wavelengths. At the same time, we elected to implement a coherent link because of its spectral and power efficiency. Coherent systems capable of achieving nearly 4 photons/bit sensitivity with QPSK modulation are currently off-the-shelf products from several vendors. The transceiver we employed has a threshold OSNR at 100Gbps of less than 13dB, and next generation transceiver already available for terrestrial deployment promises an OSNR threshold of better than 11dB. A 16QAM dual polarization link over a 50-GHz channel spacing offers a spectral efficiency of nearly 4 bits/Hertz. With such a technology, the backbone data rate can increase with traffic demand, subject only to the available power and mass constraints.

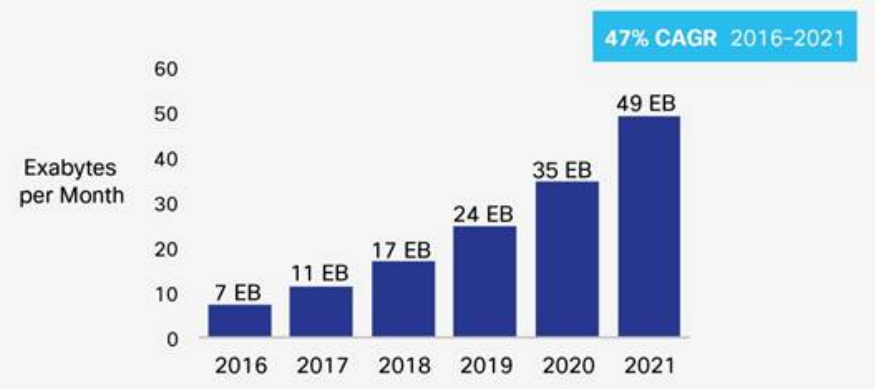

Figure 1. Global mobile traffic growth as forecasted by Cisco [1] that shows continued demand growth for data traffic..

2.1 Air-Air Link Design

We scaled the system design for an eventual 250-km range air-air link. The link budget for such a link is shown in Table 1 below. Using 1 W of transmit power and a 7.5-cm aperture with a diffraction limited beamwidth, the link can operate at a range of 250 km with better than 14 dB of link margin. The large link margin guards against scintillation fades which can occur at long link range even the design altitude when the middle part of the link dips into the tropopause where higher turbulence-induced fades can be expected.

2.2 Air-Ground Link

While the baseline of the link design is based on an UAV air-air link operating in the stratosphere, initial testing and functional demonstration of the link was conducted between a lower flying aircraft (Cessna 310) and a ground station. These two platforms provide fairly different operating environment. For example, most stratospheric low-speed platforms have low structural resonance frequencies of roughly 1 Hz and relatively low-speed propellers. The Cessna used in this demonstration has a dominant propeller mode at around 40 Hz plus strong structural components up to 200 Hz. Also, unlike the stratospheric UAV platforms that fly at approximately 10 m/s equivalent air speed (EAS), the Cessna platform that we used for the air-to-ground test flies at a minimum indicated airspeed of around 110 knots. This translates to an EAS greater than 30 m/s. The aerodynamic force scales quadratically with velocity, so the expected wind loading forces on the gimbal will be almost ten times that of the design value. To partially compensate for this, we recess the gimbal by about 6" within the airframe during this test. This configuration limits the field of regard of the gimbal to approximately +/-70 degrees from nadir. At the same time, since the air-ground link at 20-km has so much excess margin, we broaden the transmit beam to 300-urad FWHM. Even with the significant

broadening, we still have significant link margin and should effectively close the link at a range of 20 km in this increased vibrational environment.

Table 1. Link budget for an air-air crosslink with a 7.5-cm diameter aperture at 250-km range.

Air-Air Link Budget			
	Value	Units	Notes
Transmit Power	30.00	dBm	1 watt
Transmit Aperture Gain	102.72	dB	7.5cm * 0.9 = 6.75cm
Tx Mode Matching Loss	-1.00	dB	
Strehl Loss	-1.52	dB	lambda/15 in Strehl in both bench and Gimbal
Transmit Optical Loss	-2.00	dB	
Tx ASE Loss	-0.27	dB	
Space Loss	-246.14	dB	250km
Atmospheric Loss	-2.00	dB	
Pointing Loss	-3.00	dB	allocation
Receive Aperture Gain	102.72	dB	Same aperture as Tx
Rx Optics Loss	-2.00	dB	
ASE loss	-0.27	dB	
Rx Strehl loss	-1.50	dB	Residual from AO compensation system
Fiber Coupling Loss	-1.00	dB	Gaussian to Flattop mode coupling loss
Loss in Fiber prior to EDFA	-1.00	dB	
Power at EDFA Input	**-26.25**	**dBm**	
EDFA NF	5.00	dB	
EDFA output OSNR	26.75	dB	
threshold OSNR	12.70	dB	
Clear Air Link Margin (dB)	**14.05**	**dB**	

Table 2. Link budget for an air-ground link at a 20-km range with a defocused transmit beam.

Air-Ground Link Budget			
	Value	Units	Notes
Transmit Power	20.00	dBm	100mW
Transmit Aperture Gain	80.40	dB	300urad beamwidth
Tx Mode Matching Loss	-1.00	dB	
Strehl Loss	-1.52	dB	lambda/15 in Strehl in both bench and Gimbal
Transmit Optical Loss	-2.00	dB	
Tx ASE Loss	-0.27	dB	
Space Loss	-224.20	dB	20km
Atmospheric Loss	-2.00	dB	
Pointing Loss	-1.00	dB	allocation
Receive Aperture Gain	111.24	dB	90% of 20cm aperture
Rx Optics Loss	-2.00	dB	
Rx Strehl loss	-0.20	dB	Residual from AO compensation system
Fiber Coupling Loss	-1.00	dB	Gaussian to Flattop mode coupling loss
Loss in Fiber prior to EDFA	-1.00	dB	
Power at EDFA Input	**-24.54**	**dBm**	
EDFA NF	5.00	dB	
EDFA output OSNR	28.46	dB	
threshold OSNR	12.70	dB	
Clear Air Link Margin (dB)	**15.76**	**dB**	

3 FLIGHT TERMINAL DESIGN

3.1 Architecture

A block diagram of the flight lasercom payload is shown in Figure 2. A gimbal optical module provides the interface from free-space optics to a single-mode fiber. We elected to implement a compact Coudé telescope with a non-orthogonal design [2]. The Coudé implementation provides greater than hemispherical coverage and allows the same design to be used for air-to-air and air-to-ground communication links. The non-orthogonal design reduces the frontal area and hence drag of the terminal to minimize its impact on the host platform. The single-mode input/output fiber from the gimbal optical module is connected to a fiber tray assembly (FTA), which includes the high-power amplifier and a receiver optical pre-amp/AGC stage. The FTA then interfaces with the optical transceiver module which provides the digital baseband interface to the network interface. We have elected to use a commercial coherent transceiver which provides 100-Gbps line rate. The system is controlled by an internally designed processor module

which interfaces with the FTA, the quad detector/TIA, FSM driver, the Gimbal motor drivers, and the focus stage drivers, referred to here as the PAT motherboard. The PAT motherboard is an Altera Cyclone V SoC based system. It was responsible for the monitor and control of the full system state machine, and all acquisition and tracking loops.

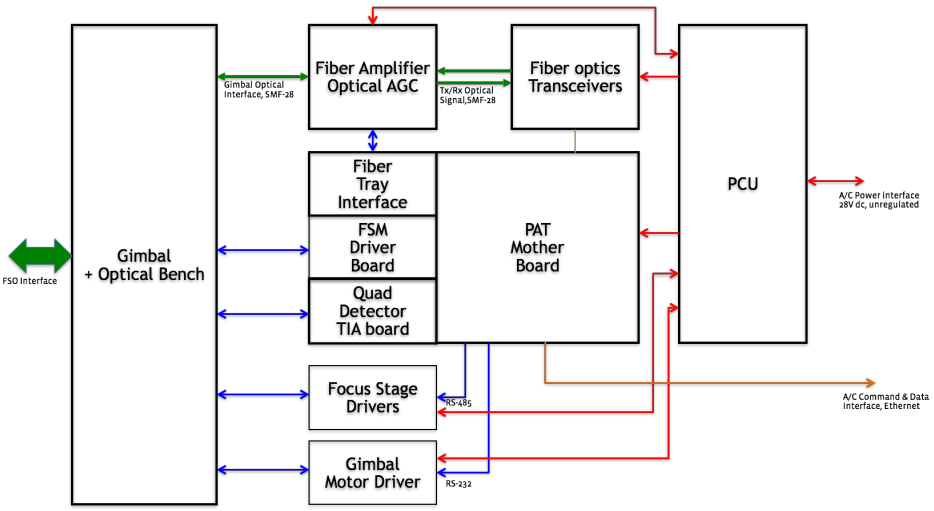

Figure 2: Block diagram of the optical crosslink payload

The optical design and completed optical gimbal telescope is shown in Figure 3 below. The telescope is a folded refractor design with 75-mm aperture, followed by a pupil relay to relay the optical signal through the Coudé path onto the small optics bench.

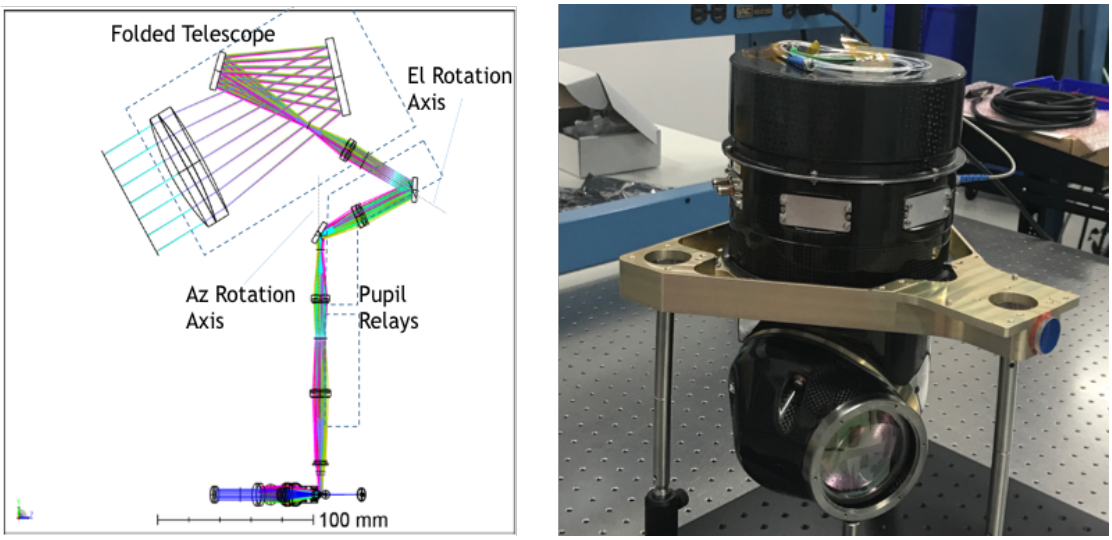

Figure 3: Optical layout of the gimbal optical module

The design of the small optics bench and the completed bench assembly is shown in Figure 4 below. A common mode fast steering mirror (FSM) stabilizes the incoming line of sight. We used a MEMS steering mirror for its lightweight, compact design. Light reflected off the steering mirror is then split off by a tracking beam splitter followed by a narrowband filter that separates the beacon wavelength (1552 nm) from the communication wavelengths (1542 and 1562 nm). A wide field of view quad provides the wide field acquisition and a narrow field quad provides the high accuracy fine tracking. To accommodate the small inter-pixel gap of the quad sensor, the wide field detector

is slightly defocused to produce a 100-um spot. The remaining part of the light is then steered by a fiber stuffing mirror and a fiber focusing lens onto the communications fiber. Both the quad focusing lens and the fiber focusing lens are mounted on motorized translation stages. This allows us to account for the temperature and altitude variation of the operating environment. An added benefit of a separate focusing stage is to allow us to defocus the fiber path and hence the communications beamwidth to account for the increased vibration environment of the Cessna flight.

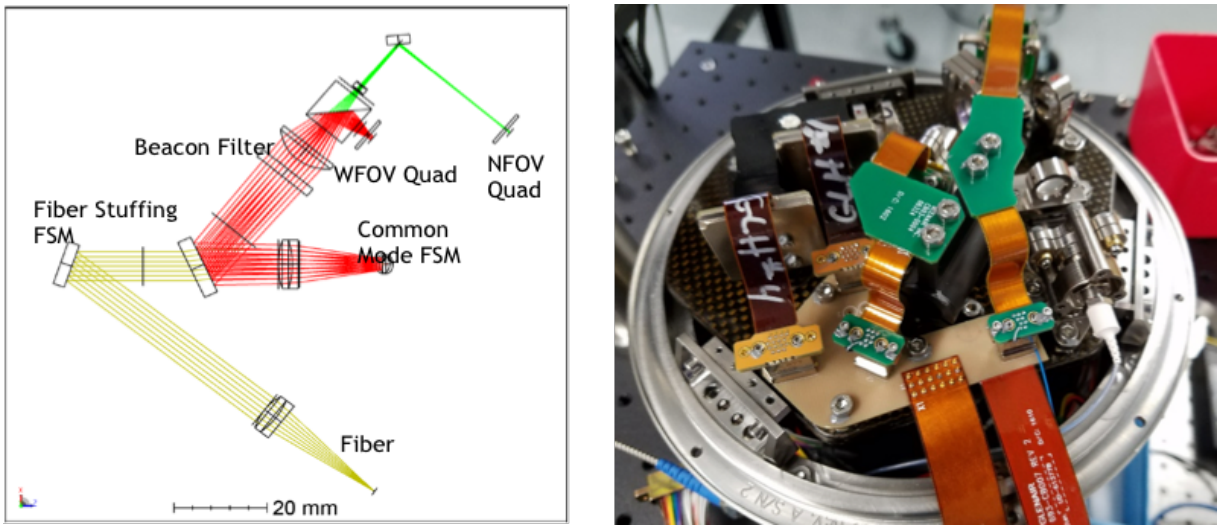

Figure 4: Optical layout of the small-space bench

3.2 Pointing and Tracking

For the air-to-ground link, the link acquisition is accomplished in several stages. In the first stage, the ground station receives the aircraft GPS location via a separate radio link and illuminates the UAV with the outer beacons. At the same time, the flight terminal points towards the ground station using ground station location and onboard GPS and inertial navigation sensor data. When the uplink beacon is detected by the flight terminal tracking sensors, the flight terminal will track and stabilize the line-of-sight and transmit downlink signal. This downlink light is subsequently acquired by a wide field-of-view boresight camera mounted on the ground gimbal, which controls the ground gimbal to ensure the downlink is within the field of view of the AO telescope. The AO system provides fine tracking and wavefront correction, and fiber coupling of this downlink light. At this point, the AO-corrected central aperture beacon light is now the dominant signal seen by the flight aperture tracking system, providing the flight terminal a more stable and intense signal to track to.

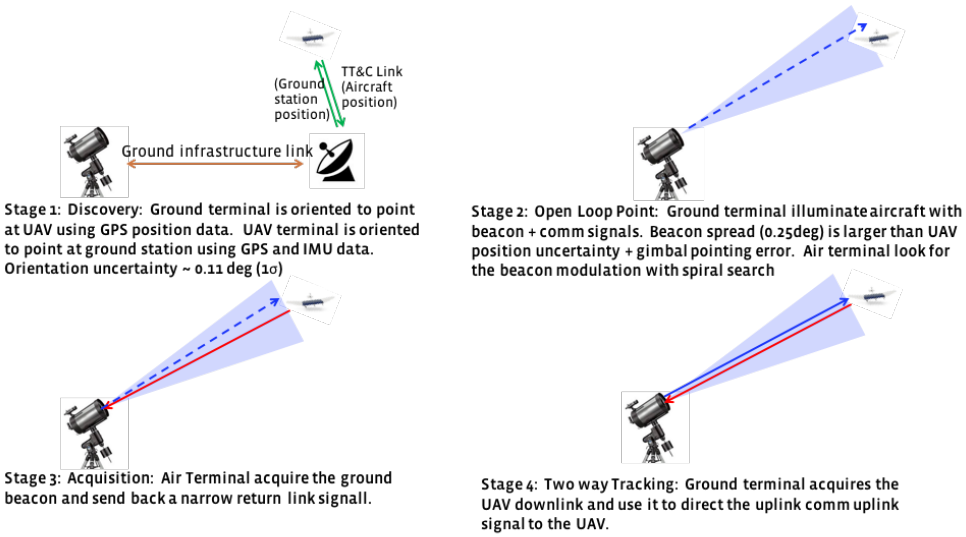

Figure 5. Spatial acquisition process for the air-to-ground link

3.2.1 Platform Jitter Characterization

Prior to the actual flight, we conducted a series of test flights intended to characterize the vibration environment of the Cessna platform. Two 6-axis sensors were mounted on the platform mounting plate and the isolated plate to characterize the base jitter and jitter on the isolation stage where the gimbal is mounted. Shown in Figure 6 are the measured PSD of the isolated stage and the residual pointing error (single axis) of the isolated and non-isolated base platform jitter, respectively. It is seen that the Cessna base produces 10 urad (rms) above 100 Hz, whereas the isolated platform reduces the high frequency jitter to 6 urad at above 100 Hz. It is seen that the isolated stage has a slightly smaller pointing error at the critical range of 100-300 Hz where the tracking loop suppression is minimum. During preparatory flights with a camera mounted in place of the small-space bench, we found that the additional line-of-sight jitter induced by wind-loading on the gimbal was substantially reduced using the isolated platform as well. Given these results, we elected to fly the gimbal on the isolated platform. The large integrated vibration power, however, indicated that a diffraction limited communications link (with a half power beamwidth of just over 20 urad), would be difficult to obtain; but a defocused gimbal with 300-urad beamwidth should easily accommodate the required tracking performance.

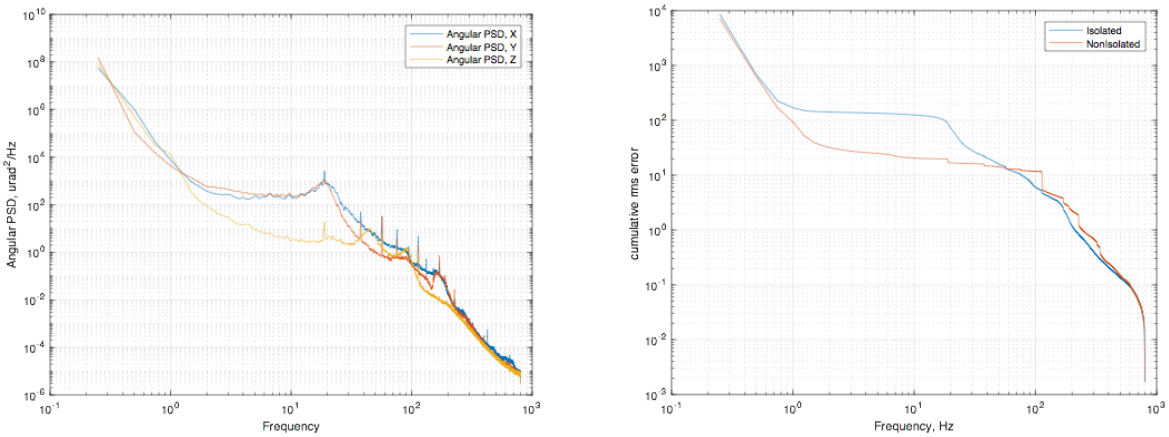

Figure 6. (Left) Measured angular PSD of the isolated platform. (Right) The leftward integral of residual rms jitter versus frequency for the isolated (red) and non-isolated (blue) platforms for the Cessna 310. The rms error above 100 Hz is 10 urad (non-isolated) and 6 urad (isolated), respectively.

3.2.2 Dynamic Pointing and Tracking

Pointing control for the flight terminal is architected as a Master-Slave control system consisting of a master Coarse pointing loop implemented in the gimbal control, plus a slaved Fine pointing loop implemented with the FSM. During tracking, persistent offsets of the Fine pointing loop are off-loaded back onto the Coarse pointing loop.

Coarse Pointing Loop
In the Coarse pointing loop, the primary goal is to point the telescope at target position (ground station) using a 2-axis gimbal referenced to a Spatial Fog IMU. Gimbal controls reject low/mid frequency band of platform vibration from aircraft and wind load induced telescope disturbance to maintain positioning the beacon within the field of view (or field of regard in worst case) on the small beam bench. In the acquisition stage, a spiral scan is added to the gimbal motion command to calibrate out uncertainties related to mechanical alignment and runtime IMU bias. At each gimbal axis of Azimuth and Elevation, the motor controller has an inner velocity loop to provide damping against bearing suspension and to attenuate inertial-based rate disturbances. In addition, an outer position loop keeps tracking of the target position commanded at 200-Hz rate. Both the velocity and position loops are shaped by conventional PID controllers plus a section of 2^{nd}-order IIR filters.

Fine Pointing Loop
The Fine pointing loop commands a Mirrorcle MEMS Fast Steering Mirror for high band suppression of input disturbance based on quad detector feedback. The beacon uplink from the ground terminal is modulated at a frequency of 76 kHz and sampled by high speed ADCs at a rate of 488 kHz. The modulation allows us to discriminate against static background glints and produces centroid measurements at 15 kHz which drives the fine pointing loop. The two main sources of input disturbances are the residual vibration left after the action of the coarse pointing loop and the atmospheric scintillation that distorted the beacon centroid measurement due to aperture intensity scintillation. The latter effect is observed when scintillation causes un-even intensity across the aperture, which shows up as centroid error on the slightly defocused wide field quad. To address the scintillation challenges, a dual quads optical design consisting of one Narrow FOV and one Wide FOV is adopted, which targets delivering better scintillation response in the area close to the Narrow FOV centroid origin while allowing for a wider acquisition range with the Wide FOV quad. A centroid blending algorithm called Centroid by Zone is proposed to simultaneously evaluate the output from two QC then combine QC signals in weights depending on the spatial zone instead of a conventional gain scheduling approach to extract the most favorable signal-over-scintillation noise ratio while minimizing the usage of saturated detector signals.

The Mirrorcle FSM, actuated by a set of electrostatic actuators, has a structural frequency response shown in Figure 7 with its first high peak resonance at 440 Hz followed by a non-minimum phase mode at 980 Hz. The signatures of input disturbance and FSM response pose significant challenges on conventional control design methods in terms of loop shaping capability to achieve the following specifics:

- High bandwidth error rejection (>100 Hz)
- Low sensitivity hump at middle frequency band (100-300 Hz)
- High loop gain (>60 dB) on low frequency (<1 Hz)
- Damping on the 1st FSM resonance mode
- Open loop roll-off before the 2nd FSM resonance mode

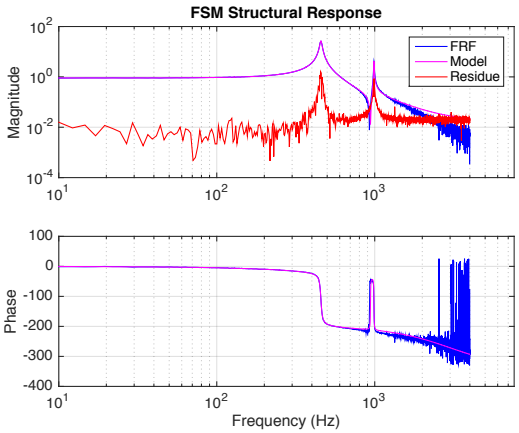

Figure 7. Open-loop response of the Mirrocle FSM used for line of sight jitter control

We used D-K synthesis to optimize the design of the controller. The result is a 24th-order controller after order reduction, the open loop response shows the achieved damping at the 440-Hz mode and robust roll-off in the vicinity of 980 Hz. The closed loop performance demonstrates a bandwidth of 120 Hz (see Figure 8) and a sensitivity peak of 3.6 dB.

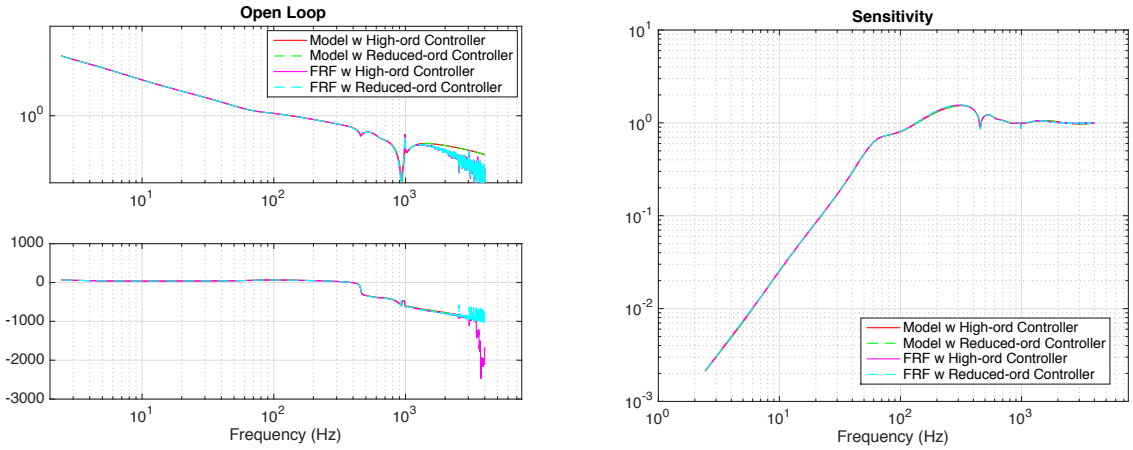

Figure 8. Closed loop response of the FSM synthesized controller

3.2.3 Static Error Calibration

In addition to the jitter rejection, accurate pointing relies on calibration of the optical system relative to the inertial reference unit to remove any static error, which consists of (a) calibration of the gimbal encoder position to absolute position reference of the mounting base, and (b) alignment between the gimbal mount and the inertial reference unit used to determine the instantaneous attitude of the platform. The first step of calibrating the beam pointing performance is via a custom designed Optical Verification System (OVS). The OVS provides a stable incoming source to the optical module and can measure the return signal wavefront and pointing jitter. Shown in Figure 9 is a diagram of the laboratory setup. The OVS also includes a counter rotating gimbal which allows testing of the flight optical gimbal in any Az-El orientation while stabilizing the actual input/output beams to the flight optical module in the laboratory frame during testing. This calibration step is first used to establish the mapping between the gimbal encoder positions and the actual angle of the Narrow FOV boresight through the gimbaled telescope relative to the mounting plate of the Gimbal and IMU.

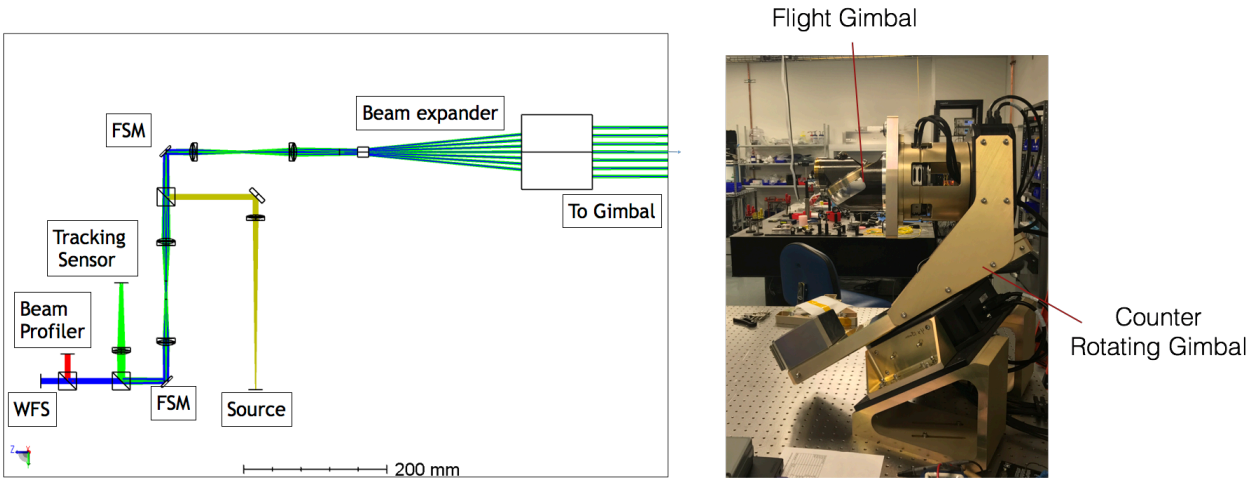

Figure 9: Optical Verification System with a counter rotating gimbal for laboratory performance characterization.

In addition to providing the gimbal pointing calibration, the OVS was also used to verify the beacon acquisition scan and FSM-to-gimbal offload performance. The outer counter gimbal was programmed to provide a simulated geometry of the actual engagement (in terms of azimuth/elevation angle of the ground station relative to the plane). At the same time, a series of simulated IMU messages was provided through the Ethernet connection to the PAT motherboard in order to spoof the location and attitude of the flight terminal. The flight software then interprets the IMU messages and initiates the acquisition scan around the preloaded ground terminal coordinates chosen here to point directly into the OVS bean expander. Once the link is acquired, the continuous motion of the outer gimbal leads to bias in the tracking mirror that must be off-loaded to the gimbal to maintain the tracking FSM near the center of its dynamic range. Testing of the bias off-load was successfully completed using the OVS and counter gimbal prior to the actual flight test.

The next step of pointing calibration (IMU to gimbal alignment) is performed after the gimbal is mounted on the airplane. From the calibration done on the OVS, the relation between the Narrow quad boresight and a frame defined by the mounting point of the IMU is known over gimbal angles. However, the IMU reports an attitude which is dependent on the exact offsets of the dual GPS antennas relative to the IMU. In order to finalize the calibration of the Narrow quad boresight to the external world in the IMU frame, we perform a single-vector alignment using a pair of Real Time Kinematic (RTK) receivers after the flight gimbal is mounted on the Cessna aircraft. RTK receivers measure the position of a GPS antenna on the aircraft and a rover receiver to cm-level accuracies. We send the collimated transmit signal from the aircraft gimbal onto a target board located 250 m from the aircraft, and by measuring the relative location between the gimbal and the target board RTK antennas, we were able to accurately deduce the relation between the gimbal reference frame and the aircraft IMU position to within the field of view of the Wide quad, approximately 2 mrad. During flights, we routinely found that this calibration procedure was accurate enough that the wide uplink beacons were already appearing on the wide Flight terminal quad once the Flight terminal was open-loop pointing towards the ground terminal.

4 GROUND TERMINAL

The ground terminal is located on a rooftop near Los Angeles, California. Shown in Figure 10 below is the block diagram of the ground terminal. The terminal is built around a 200-mm aperture adaptive optics (AO) telescope and the beacon launch optics. The AO telescope and the beacon launch optics are mounted on a Az-El gimbal housed in a weather protected dome. A rotating cable tray assembly allows the gimbal to rotate up to +/-270 degrees. A picture of the assembled rooftop dome is shown in Figure 11. The main control terminals for the AO telescope, the beacon and communications optical fiber amplifiers, the transceivers, as well as the traffic generators and data recorders are housed in a separate control room within the main building.

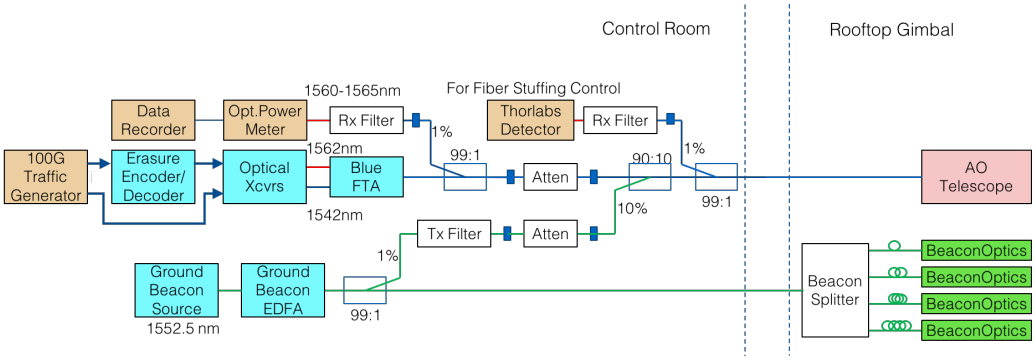

Figure 10: Block Diagram of the ground terminal

Figure 11: Rooftop dome assembly consisting of the AO telescope, the Alt-Az gimbal, and the beacon launch optics.

4.1 Adaptive Optics Telescope

The AO system corrects the incoming signal wavefront so that it can be more effectively coupled into a single-mode fiber. Since the channel is reciprocal between the two single-mode-fiber end points, improved coupling into the fiber also provides fade mitigation on the flight terminal end of the link. A block diagram of the AO telescope is shown in Figure 12. Incoming light is collected by the 200-mm aperture telescope. A fast steering mirror slaved to a tracking camera corrects the line of sight error of the incoming light and removes any residual tip-tilt to fit within the dynamic range of the wavefront sensor. A MEMS deformable mirror then corrects the higher-order wavefront error. An aperture sharing element (ASE) splits off most of the incoming signal toward the fiber stuffing assembly. The remaining signal is then detected by a wavefront sensor (WFS) which feeds the control loop driving the DM, and a scoring camera that measures the effective Strehl of the corrected beam.

The fiber stuffing path consists of a piezo-actuated tip-tilt mirror and a motorized focusing stage. Fiber power peaking is accomplished by nutating the tip-tilt mirror to sense the line of sight error between the comm fiber and the WFS while the focusing stage is dithered to find the optimum focus for fiber coupling.

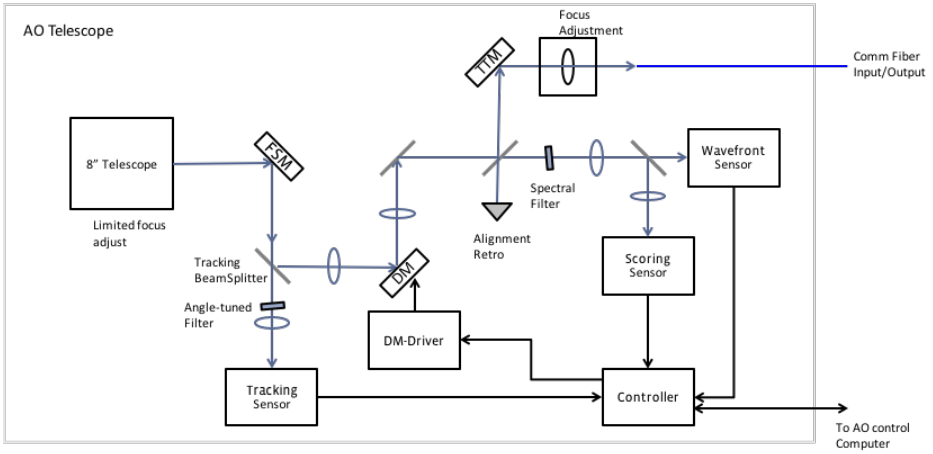

Figure 12: Adaptive Optics Telescope Assembly

4.2 Multiple-Beacon Launch Optics

Fade mitigation on the tracking path is achieved using multiple uplink beacons. We use a multi-aperture beacon in a '4 plus 1' configuration: the main telescope aperture is surrounded by 4 small-aperture beacon launches separated by an average of 300 mm which is larger than the largest expected operational r_0 to ensure spatial diversity of the uplink beacon paths. These beacons are fed from a single broadband source with path lengths to each aperture differing by 10's of cm to ensure mutual non-coherence between different aperture signals. A small portion of the beacon light is picked off from the source and combined in fiber with the uplink communication signal just before the coupling to free-space. The ratio of powers between the 4-aperture and central aperture beacons is chosen such that the intensity of beacon light arriving at the flight terminal from the central aperture is approximately 20 dB higher than that of the outer beacons. In this way, the flight terminal can find first signal on the broad beacon for acquisition and then track on the AO-corrected light from the central aperture which is co-boresighted with the comm signal as shown in Figure 10.

4.3 Link Protection

For communications under scintillating channels, the terminal includes the use of a packet erasure code to provide fading protection [3]. We use a specific implementation of a packet erasure code developed in collaboration with Qualcomm Technologies, Inc. The concept of an erasure coded channel is illustrated in Figure 13 below. More specifically, a packet erasure code (Qualcomm® RaptorQ™ code) was selected to enable the use regenerative encoding without the need to decode at each hop of the network. This is particularly useful in a multi-hop airborne backbone as additional repair data can be added at each hop and decoding only needs to happen at the end point (e.g. on the ground where the user data is recovered) and thus reduces the need for carrying the mass and power consumption of a high rate decoder. Initially, the decoders are implemented using software (used in the current demo). The code is designed to provide a variable code rate from 0.2 to 0.8 and a protection period between 20 and 125 ms.

Since the link is reciprocal thanks to the negligible point-ahead angle and single-mode fiber on both ends of the link, we also implemented a simple retransmission scheme for link protection. Every time a link fault is detected, the transmitter will jump back to resend pre-set number of packets once the link was restored. This scheme proved to be effective for short-duration faults.

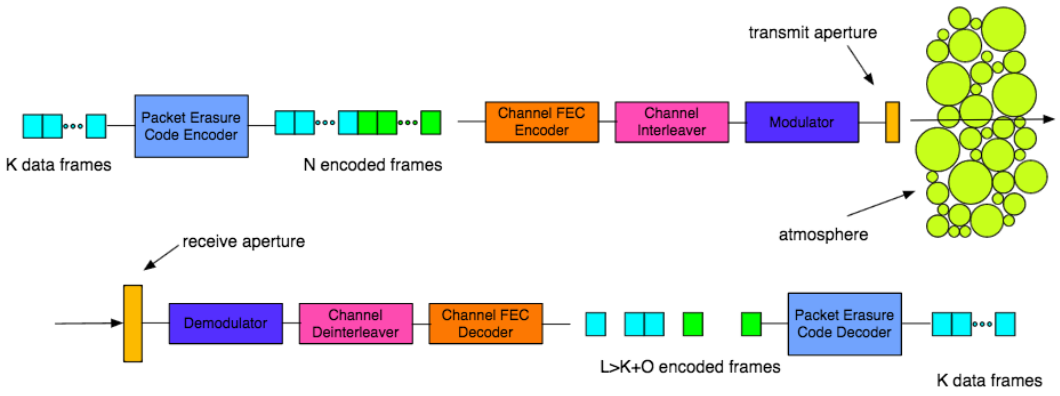

Figure 13. Packet erasure code for end-end link protection

5 COMMUNICATIONS LINK TESTS

Prior to actual flight testing with the Cessna aircraft, we conducted an end-end link test in the laboratory using a Fresnel-scaled geometry. The setup of the test is shown in Figure 14. The output of the terminal is telescoped down to small-beam space where the beams propagate through pseudorandom phase screens and a distance such that the paraxial beam expansion losses match what is expected in the field. We chose a transverse scaling of 62.5:1, which in turn results in a 3900:1 scaling in the pathlength, allowing us to fit an effective 16-km pathlength into 4 m on a standard optical table. Pseudorandom phase screens following a Kolmogorov spectrum from Lexitek Inc. are used to simulate the effect of turbulence [4], and a jitter injection mirror in the small beam path allows us to inject simulated vibration condition into the optical input to the flight terminal to verify that we can effectively track the ground uplink in the presence of the vibration.

We tested the 16-km link with a simulated C_n^2 profile that is based on the H-V 5/7 profile with a multiplier of 12.5 and engagement angle of 60° from zenith. This placement should result in an r_0 of 2.5 cm at the AO input aperture, which, in addition to the Kolmogorov spectrum, is verified by reconstructing the incoming wavefront phase structure function from the AO closed-loop command data. The scaled geometry test verified that we can close a coherent communications link through turbulence.

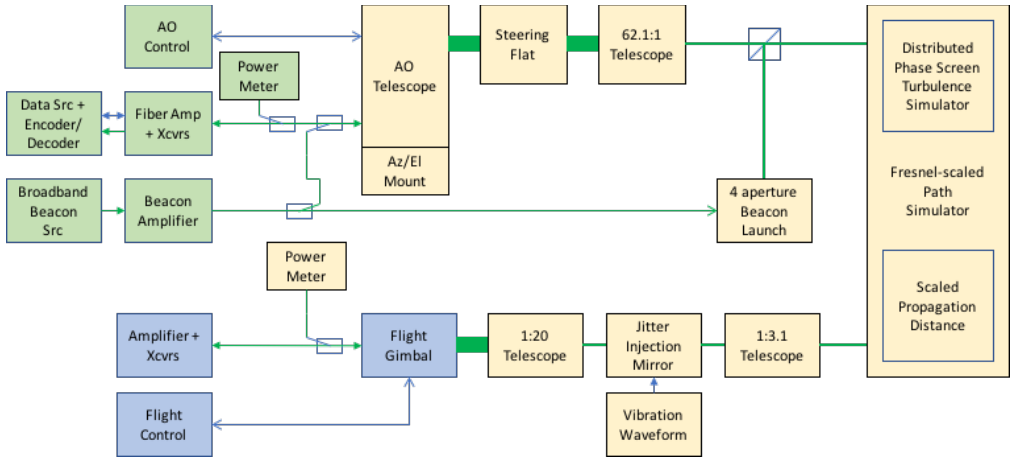

Figure 14. Propagation test lab used to verify the link performance

Subsequent to the lab test, we completed a series of successful flight tests using a Cessna 310 aircraft. The payload mounting plate is attached to mounting flange on the airframe and has a direct view of the ground at up to +/-70 degrees from nadir. The payload mounting plate houses the flight gimbal and electronics (pointing controller, transceiver, gimbal driver, etc.). The electronic components are cooled via a liquid cooler sold as a CPU heat exchanger which could be replaced with cooling through the UAV skin at altitude.

Shown in Figure 15 is the configuration of the payload. The gimbal was mechanically isolated form the aircraft using three elastomeric isolators. Our earlier tests had shown that such configuration reduces the high frequency jitter compared to hard mounting the gimbal to the airframe (Figure 6). An inertial reference unit (Spatial FOG) was also mounted on the isolated stage to provide attitude reference for pointing the gimbal. The Spatial FOG uses differential GPS fed by two antennas mounted on the top-side of the aircraft to provide heading information, while pitch and roll are measured directly by the Spatial FOG unit. Communications to the ground station is provided by a separate radio link which permits monitor and control of the payload from the ground.

Figure 15. Configuration of the payload on the aircraft

During the flight tests, the aircraft is generally flying at 17,500 ft in a circle centered on the ground terminal at a nominal range of 10-20 km to our ground station (Figure 16). At this altitude, the 310 could only safely maintain 110 kts as a minimum indicated airspeed. This flight path gives a continuous contact period of around 15 minutes before hitting a point where the sun enters into the safety zone of the ground terminal line-of-sight or the ground terminal cable carrier tray must be unwrapped. We conducted flight tests over both nighttime and daytime conditions, and Figure 17 shows some of the results during two flights. Given that the system threshold is around -40 dBm, we found that the link is generally maintained with >10 dB link margin. As an example at 22.5 h on the left hand plot in Figure 17, the bit error rate reported by the transceivers after loopback was typically $8{\cdot}10^{-7}$ to $2{\cdot}10^{-6}$. During the same time, the datastream protected with the packet erasure code reported no packet errors aside from burst loss events of 100-3000 packets, which occurred with a frequency of roughly 25 times over 10 minutes of engagement. These burst loss events were correlated with drops in in-fiber power due to a combination of atmospheric-induced deep fades and rapid airplane attitude adjustments by the pilot.

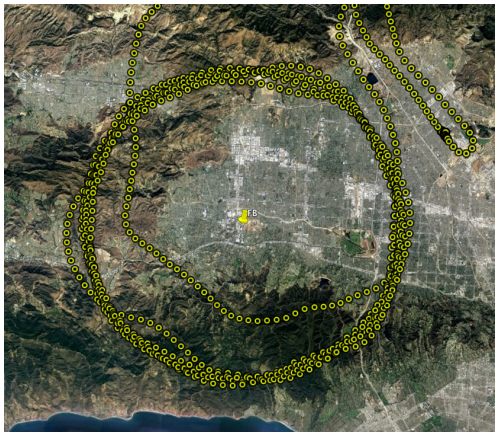

Figure 16. Typical flight path during the flight test is a circular flight pattern

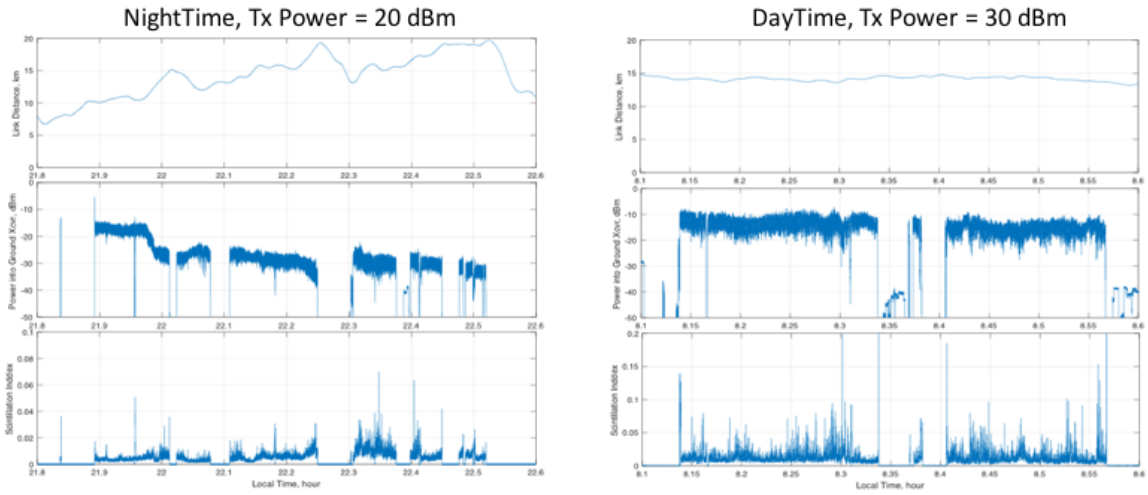

Figure 17. Flight test showing link closure for nighttime (left) and daytime conditions (right) on the downlink receive channel.

6 SUMMARY AND NEXT STEP

We presented a summary of the flight demonstration of an air-ground coherent optical link over a link range of 10-20 km. Using commercial, off-the-shelf coherent optical transceivers, the link operated at a line rate of 100 Gbps, bidirectionally, with a threshold received optical power level of less than -40dB. The adaptive optics ground terminal, located on the rooftop in an urban environment, successfully operated over both day- and nighttime conditions. To account for the added aircraft vibration environment of a low flying Cessna aircraft, the transmit signal from the airborne terminal is broadened to an angular divergence of ~300 urad. This large angular beamwidth is sufficient to accommodate the vibration environment and results in a stable optical link between the Cessna aircraft and the ground station. Link analysis and the demonstration show that there is sufficient link margin at the link range even at this level of beam divergence.

As a proof of concept demonstration, this flight test demonstrated the feasibility of designing a light-weight terminal for UAV applications. The two-axis gimbal, weighing just over 3 kg, can support both air-air and air-ground engagement with more than hemispherical field of regard. The electronics, consists of several units (monitor and control, fiber amplifiers, transceiver and network interfaces, gimbal and translation stage drivers) weighs just over 5 kg, not including flight harnesses. The flight system power consumption is around 150 W. The mass and power of the electronics can be further reduced with next generation transceivers and improved packaging. The current gimbal

design employs a single fiber to provide transmit and receive signal interface. This is adequate for air-air and air-ground connectivity applications where the point ahead angle is much smaller than the beamwidth. For air-satellite connectivity, where the point ahead angle is typically larger than the beamwidth, a separate point ahead mechanism with separate transmit-receiver fiber interfaces will be required. We have also explored alternative architectures to support a separate transmit point ahead function [5] as an option for future design evolution.

7 REFERENCES

[1] Cisco Visual Networking Index: Global Mobile Data Traffic Forecast Update, 2016–2021 White Paper. From https://www.cisco.com/c/en/us/solutions/collateral/service-provider/visual-networking-index-vni/mobile-white-paper-c11-520862.html

[2] A. Talmor, H. Harding, and C. Chen, "Two-axis gimbal for air-to-air and air-to-ground laser communications," in *Free-Space Laser Communication and Atmospheric Propagation XXVIII, 97390G (15 March 2016);* , San Franscisco, 2016.

[3] W. Zhang, S. Hranilovic, C. Shi, "Soft-switching hybrid FSO/RF links using short-length raptor codes: design and implementation," *IEEE Journal on Selected Areas in Communications,* vol. 27, no. 9, p. 1698, 2009.

[4] J. D. Schmidt, Numerical Simulation of Optical Wave Propagation, Bellingham, WA: SPIE Press, 2010.

[5] E. Miller, et.al., "Fine Pointing and Tracking Concepts for Optical Intersatellite Links," in IEEE International Conference on Space Optical Systems and Applications, Okinawa, JP, 2017.